

Nanomechanical studies of the compressive behavior of carbon fibers

Melanie Todt · Franz G. Rammerstorfer ·
Oskar Paris · Franz D. Fischer

Received: 23 August 2010/Accepted: 18 September 2010/Published online: 2 October 2010
© Springer Science+Business Media, LLC 2010

Carbon fiber reinforced plastics (CFRP) are subjected to compressive or bending loading in many structural applications. The mechanical behavior of the CFRP in the compressive range depends on the mechanical behavior of the carbon fibers. Thus, the compressive behavior of carbon fibers is of great interest and investigated in many articles see, e.g., [1–5]. The nano-structure of the carbon fibers is formed by so called carbon crystallites [2, 6–9], i.e., stacks of imperfect graphene layers. In [2] the influence of structural properties, like crystallite size and crystallite orientation, on the compressive behavior of carbon fibers is investigated using X-ray diffraction. Furthermore, it is assumed that carbon fibers fail by the occurrence of crystallite buckling. The non-Hookean behavior of fibers tested using the loop test is also related to buckling of the carbon crystallites [1]. The occurrence of crystallite buckling in fibers subjected to compressive loading is also assumed in [4, 5]. Experimental proof of this assumption is found in

[8], where crystallite buckling of fibers is directly observed using microbeam X-ray diffraction. In the present study, the compressive behavior of single carbon crystallites is investigated using the finite element method. The aim is to better understand the influence of crystallite buckling on the overall compressive behavior of the fibers.

Carbon crystallites are planar structures consisting of a number of graphene layers of finite extension, see Fig. 1. In the present study, it is assumed that the graphene planes are all oriented parallel to the fiber axis and that the crystallite consists of about eight layers which is typical for polyacrylonitrile (PAN) based carbon fibers. As depicted in Fig. 1, the carbon atoms forming the layers are arranged in a hexagonal lattice and interact via van der Waals (vdW) forces with atoms on neighboring layers. The reported equilibrium distances between two graphene layers in carbon fibers range from $d_{002} = 0.344$ to 0.356 nm in [7] or $d_{002} = 0.339$ to 0.347 nm in [4], depending on the fiber type. In the present study, an equilibrium distance of $d_{002} = 0.34$ nm is assumed, which is in good agreement with the above values. Furthermore, the size of the layers L_a is assumed to be approximately 4 nm, which is also in good agreement with values reported for PAN-based fibers, see [2] and [4]. Graphene layers forming the crystallite contain defects such as vacancies which can lead to a formation of covalent interlayer bonds between neighboring layers [10]. Furthermore, dangling bonds at the edges of the individual graphene layers have to be saturated [11] which may also lead to the formation of covalent interlayer bonds. In the present study, it is assumed that the occurring interlayer bonds at the edges and within the crystallite are similar and reduce the interlayer distance locally to $d_c \approx 0.258$ nm which corresponds to the distance reduction reported for a fourfold coordinated interstitial atom as shown in [10] by ab-initio DFT calculations.

M. Todt (✉) · F. G. Rammerstorfer
Institute of Lightweight Design and Structural Biomechanics,
Vienna University of Technology, Gusshausstrasse 27-29,
1040 Vienna, Austria
e-mail: mt@ilsb.tuwien.ac.at

F. G. Rammerstorfer
e-mail: ra@ilsb.tuwien.ac.at

O. Paris
Institute of Physics, Montanuniversität Leoben,
Franz-Josef-Straße 18, 8700 Leoben, Austria
e-mail: Oskar.Paris@unileoben.ac.at

F. D. Fischer
Institute of Mechanics, Montanuniversität Leoben,
Franz-Josef-Straße 18, 8700 Leoben, Austria
e-mail: Mechanik@unileoben.ac.at

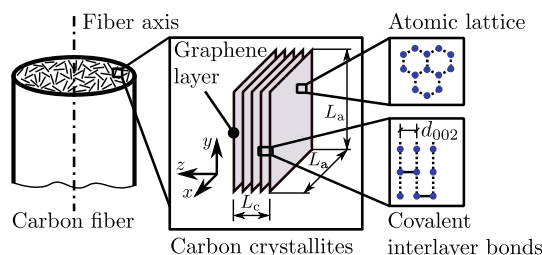


Fig. 1 Nanostructure of PAN-based carbon fibers

The finite element model is based on a hybrid continuum mechanics—discrete atomistic approach. The layers are discretized using linear shell elements with thickness $h = 0.066$ nm, elastic modulus $E = 5.5$ TPa, and a Poisson's ratio of $\nu = 0.19$, resulting from molecular dynamic simulations, see e.g., [12]. In [12] E , ν , and h are derived for carbon nanotube walls and must be considered as virtual values leading not only to a correct membrane stiffness [13] but also to a correct bending stiffness [14] for graphene layers, the latter not being considered in [13]. The vdW interactions between the layers are modeled using a pressure distance relation derived for graphite [15]. The vdW interactions are implemented as user interface in ABAQUS¹, assuming zero shear stiffness of the interface [16]. Two different models are investigated according to possible locations of covalent interlayer bonds. The covalent interlayer bonds are distributed either randomly within the crystallite (model M1) or randomly along the edges (model M2) only, assuming defect free graphene layers. To assure that the minimum distance between two bonded atoms within one layer is equal to the carbon-carbon bondlength, the hexagonal atomic lattice is mapped to the finite element mesh by defining so called “atom nodes” at the atom positions. In the present study, AA stacking of the graphene layers is assumed leading to the same discretization for all layers. According to [17], AA stacking is energetically less favorable than AB (graphite) stacking. However, the energy difference between these two configurations is rather small [18], so that the assumption of AA stacking seems reasonable. Two directly opposite “atom nodes” of neighboring layers can be connected by covalent interlayer bonds, which is a rough approximation of the bonding configuration reported in Fig. 3 in [10]. The interlayer bonds are modeled as single trusses (no bending or torsional stiffness) with an initial length of $d_c = 0.34$ nm and with a tensile stiffness much higher than the membrane stiffness of the layers. To reduce the length of the bonds from 0.34 to 0.258 nm they are subjected to a virtual temperature change ΔT in an initial step. The axial compression is applied in a second step via prescribed displacements to the upper edge of the crystallite in

negative y -direction. Carbon fibers have usually diameters in the range of 1 to 10 μm , which is much larger than the crystallite dimensions perpendicular to the fiber axis ($\approx 4 \times 2.5$ nm). Thus, the microstrain [8] in bending can be assumed to be constant over the crystallite's dimensions. The boundary conditions for the initial, i.e., thermal step and the loading step are depicted in Fig. 2 left and right, respectively. In both steps it is assumed that the y -axis of the crystallites is parallel to the fiber axis. The zero shear stiffness of the vdW interface and the simplified truss model of the interlayer bonds lead to a zero shear stiffness between neighboring layers. To avoid rigid body modes in form of a shearing-off of individual layers rather restrictive boundary conditions are required, especially for the initial step. Experimental results, see [7], show that the effective in-plane shear modulus is only about 1.2% of the effective axial elastic modulus. Thus, the zero shear stiffness between the layers should have no major influence on the occurrence of crystallite buckling.

The shrinkage of the interlayer bonds in the initial step introduces displacements and self-equilibrating stresses into the crystallites. Due to this displacements inclinations of the layers at the upper and lower edges of the crystallite χ_U and χ_L appear, respectively (Fig. 3b). As depicted in Fig. 3 the displacements after the initial step strongly depend on the location of the covalent interlayer bonds. In M1 the covalent interlayer bonds lead to local dimples in the layers only (Fig. 3a), and the inclinations are very small ($\chi_U, \chi_L < 1^\circ$) and independent of the amount of interlayer bonds. For M2 a pre-bending deformation in the form of an overall bulging of the crystallite can be observed, see Fig. 3b and local dimples form at the edges of the crystallite. χ_U and χ_L depend slightly on the amount of covalent interlayer bonds and are about 4° which is much smaller than the values measured in [8] which are around 11° . However, in [8] a total misalignment is measured which maybe is a superposition of a pre-bending deformation due to the formation of covalent interlayer bonds and a general misalignment of the crystallites, which is not captured with the current model. Graphene sheets also exhibit a certain waviness [19] which is not taken into account here. Interlayer bonds in the

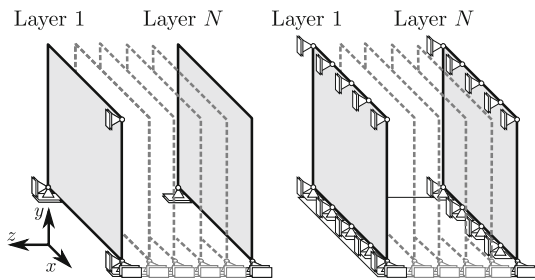


Fig. 2 Boundary conditions applied for step 1 (left) and step 2 (right), respectively

¹ http://www.simulia.com/products/abaqus_fea.html.

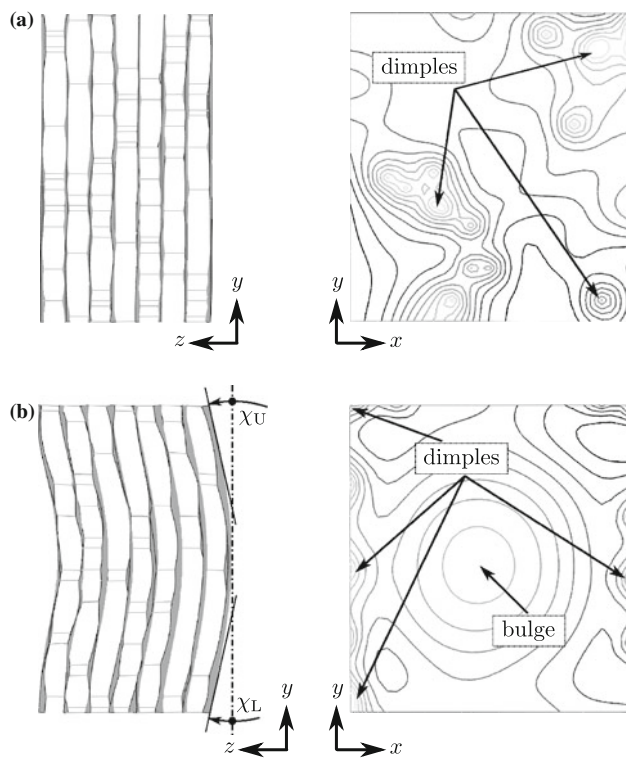


Fig. 3 Deformation states after the initial step for models M1 (a) and M2 (b). The side view of the deformation state and the contour lines of the z -displacements of the uppermost layer are depicted on the left side and on the right side, respectively

interior of the crystallite (M1) have a supporting effect and thus, bending induced distance reductions as observed in the bulge area of M2 are prevented.

The different deformation states of M1 and M2 after the initial step lead to a difference in their compressive behavior. The load–displacement diagrams of the compressive analysis of M1 and M2 are depicted in Fig. 4. For a parametrical study the amount of covalent interlayer bonds is varied from 1 to 5% bonded atoms for both, M1 and M2. For M1 the axial compressive force F_y depends linearly on the applied displacement u_y until buckling of the crystallite occurs. The critical compressive force F_y^* and the critical displacement u_y^* at the onset of buckling increase significantly with the amount of covalent interlayer bonds. The tangential stiffness $\hat{K}_T = \frac{dF_y}{du_y}$ in the pre-buckling regime is larger than the tangential stiffness in the post-buckling regime. However, in both regimes the tangential stiffness is almost independent of the amount of interlayer bonds. If the covalent interlayer bonds are only distributed at the edges of the crystallite (M2) the substantial pre-buckling deformation after the initial step leads to a nonlinear response of the crystallite already for small displacements u_y . For M2 the amount of interlayer bonds has no significant influence on the compressive response

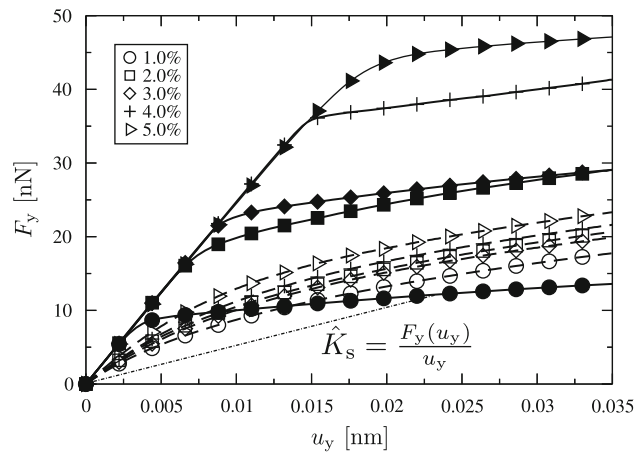


Fig. 4 Load-displacement diagram for different amounts of covalent interlayer bonds ranging from 1 to 5% bonded atoms (M1 continuous lines with full symbols, M2 dashed lines with open symbols)

(see Fig. 4) and thus, on the tangential stiffness. The results show that randomly distributed interlayer bonds within the crystallite have a stabilizing effect whereas interlayer bonds located only on the edges have a de-stabilizing effect due to large pre-buckling deformations. In both cases the tangential stiffness is not influenced by the amount of interlayer bonds.

The effective axial secant modulus \hat{E}_S of a crystallite can be evaluated from the secant stiffness \hat{K}_S (see Fig. 4) using $\hat{K}_S = (\hat{E}_S A)/(l)$ with $A = L_a \times L_c$ as the initial cross section and $l = L_a$ as the initial height of the crystallite, see Fig. 1. If the covalent interlayer bonds are randomly distributed within the crystallite (M1) the secant modulus \hat{E}_S is equal to the tensile modulus of the crystallite and remains almost constant until buckling occurs, see Fig. 5. After buckling of the crystallite \hat{E}_S decreases significantly, where the decrease is stronger for a low amount of interlayer bonds. For (M2) a constant region of \hat{E}_S , cannot be observed, due to large pre-buckling deformations. The initial value of \hat{E}_S is much lower than for M1 but is also not significantly influenced by the amount of covalent interlayer bonds. With the assumed elastic properties (E, v) and the assumed layer thickness (h) the bending stiffness of the layer can be calculated as $D = \frac{E h^3}{12(1-v^2)} = 0.137 \text{ nNm}$, which is in good agreement with values given in [14]. However, the so called dihedral angle effect is not considered here. Considering this effect results in $D = 0.225 \text{ nNm}$ [14], which is much larger than the above assumed value. Nevertheless, the initial values of \hat{E}_S , simulated with M1 and ranging from 1,105 to 1,158 GPa, are in good agreement with the experimental values of $1,140 \pm 10 \text{ GPa}$ reported in [7]. This gives some evidence, that the formation of the covalent bonds occurs randomly within the crystallite and not only at the edges.

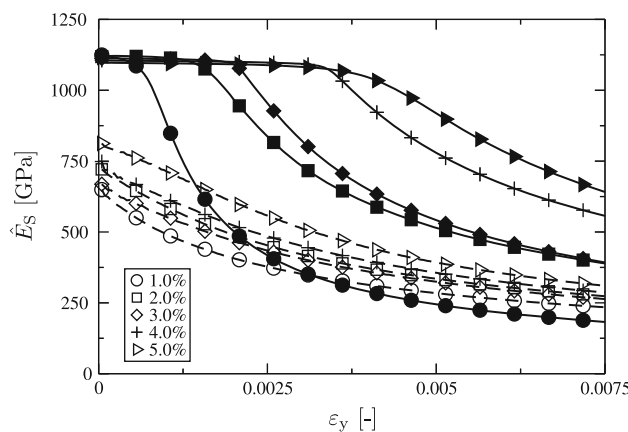


Fig. 5 Secant moduli \hat{E}_S for different amounts of covalent interlayer bonds ranging from 1 to 5% bonded atoms (M1 continuous lines with full symbols, M2 dashed lines with open symbols)

The current model confirms assumptions made in [2, 5] and experimental observations made in [8]. The obtained initial effective axial secant modulus of the crystallites is in good agreement with values reported in literature, see e.g., [7], and the reduction of the axial secant modulus after the occurrence of buckling gives an explanation for the difference between the tensile and the compressive behavior of carbon fibers. Nevertheless, two main simplifications are made in the current crystallite model. First, the covalent interlayer bonds are modeled as trusses (with no bending or torsional stiffness) connecting two directly opposite “atom nodes” of the finite element mesh. This is as strong simplification of the interlayer bond configurations reported in [10]. Second, the boundary conditions are rather artificial due to the zero shear stiffness between neighboring layers and the lack of information about interactions between neighboring crystallites. To obtain a more realistic characterization of the compressive behavior of carbon crystallites improvements in the modeling of the interlayer bonds and the boundary conditions are necessary.

In summary, in the present study the compressive behavior of carbon crystallites forming the nano-structure of PAN-based carbon fibers is investigated by a hybrid continuum mechanics-atomistic model using the finite element method. The load displacement response and the effective axial secant modulus of crystallites are obtained. It is shown that the effective axial secant modulus is

significantly reduced after the onset of crystallite buckling. The occurrence of buckling is influenced by the location of the covalent interlayer bonds as well as by their amount. Covalent interlayer bonds randomly distributed within the crystallite have a stabilizing effect whereas covalent interlayer bonds distributed only at the edges de-stabilize the crystallite due to significant pre-buckling deformations. The derived simplified models and results can serve as a basis for a homogenization analysis required to calculate the stiffness properties of carbon fibers.

Acknowledgements The first author, Melanie Todt, is grateful for funding provided by the fFORTE WIT—Women in Technology Program of the Vienna University of Technology, and the Austrian Federal Ministry of Science and Research.

References

1. Hawthorne H (1993) J Mater Sci 28:2531. doi:[10.1007/BF01151688](https://doi.org/10.1007/BF01151688)
2. Dobb MG, Guo H, Johnson DJ, Park CR (1995) Carbon 33:1553
3. Oya N, Johnson DJ (1999) Carbon 37:1539
4. Oya N, Johnson DJ (2001) Carbon 39:635
5. Nakatani M, Shioya M, Yamashita J (1999) Carbon 37:601
6. Paris O, Peterlik H (2009) In: Eichhorn S, Hearle JWS, Jaffe M, Kikutani T (eds) Handbook of textile fibre structure. Woodhead Publishing Ltd, Abington
7. Loidl D, Peterlik H, Müller M, Riekel C, Paris O (2003) Carbon 41:563
8. Loidl D, Paris O, Burghammer M, Riekel C, Peterlik H (2005) Phys Rev Lett 95: 225501
9. Loidl D, Paris O, Rennhofer H, Müller M, Peterlik H (2007) Carbon 45:2801
10. Telling RH, Ewels CP, El-Barbary AA, Heggie MI (2003) Nat Mater 2:333
11. Vollath D (2008) Nanomaterials. Wiley, Weinheim
12. Yakobson BI, Brabec CJ, Bernholc J (1996) Phys Rev Lett 76:2511
13. Van Lier G, Van Alsenoy C, Van Doren V, Geerlings P (2000) Chem Phys Lett 326:181
14. Lu Q, Arroyo M, Huang R (2009) J Phys D 42:102002
15. Kelly B (1981) Physics of graphite. Applied Science Publishers, London
16. Yao X, Han Q, Xin H (2008) Comput Mater Sci 43:579
17. Charlier JC, Michenaud JP (1992) Phys Rev B 46:4531
18. de Andres PL, Ramirez R, Verges JA (2008) Phys Rev B 77:045403
19. Meyer JC, Geim AK, Katsnelson MI, Novoselov KS, Booth TJ, Roth S (2007) Nature 446:60